Efficient water oxidation catalyzed by homogeneous cationic cobalt porphyrins with critical roles for the buffer base

Dong Wang and John T. Groves[1]

Department of Chemistry, Princeton University, Princeton, NJ 08544

Contributed by John T. Groves, August 14, 2013 (sent for review July 4, 2013)

A series of cationic cobalt porphyrins was found to catalyze electrochemical water oxidation to O_2 efficiently at room temperature in neutral aqueous solution. Co–5,10,15,20-tetrakis-(1,3-dimethylimidazolium-2-yl)porphyrin, with a highly electron-deficient *meso*-dimethylimidazolium porphyrin, was the most effective catalyst. The O_2 formation rate was 170 nmol·cm^{-2}·min^{-1} (k_{obs} = 1.4 × 10^3 s^{-1}) with a Faradaic efficiency near 90%. Mechanistic investigations indicate the generation of a Co^{IV}-O porphyrin cation radical as the reactive oxidant, which has accumulated two oxidizing equivalents above the Co^{III} resting state of the catalyst. The buffer base in solution was shown to play several critical roles during the catalysis by facilitating both redox-coupled proton transfer processes leading to the reactive oxidant and subsequent O–O bond formation. More basic buffer anions led to lower catalytic onset potentials, extending below 1 V. This homogeneous cobalt-porphyrin system was shown to be robust under active catalytic conditions, showing negligible decomposition over hours of operation. Added EDTA or ion exchange resin caused no catalyst poisoning, indicating that cobalt ions were not released from the porphyrin macrocycle during catalysis. Likewise, surface analysis by energy dispersive X-ray spectroscopy of the working electrodes showed no deposition of heterogeneous cobalt films. Taken together, the results indicate that Co–5,10,15,20-tetrakis-(1,3-dimethylimidazolium-2-yl)porphyrin is an efficient, homogeneous, single-site water oxidation catalyst.

electrocatalysis | oxygen | photosynthesis | high valent | single site

Water oxidation is a key step in photosynthesis that efficiently harvests and stores solar energy (1). The oxidation of H_2O to O_2 is a four-electron, four-proton process in which O–O bond formation is the key chemical step. In photosystem II, these proton-coupled electron transfers (PCETs) occur via a tyrosine at the Mn_4Ca oxygen-evolving complex (2). An important thermodynamic aspect of photosynthesis is the efficient conversion of photonic energy to electrical potential, thus providing 99% of the driving force required to convert CO_2 to carbohydrates (Eqs. **1** and **2**):

$$6\ CO_2 + 6\ H_2O \rightarrow C_6H_{12}O_6 + 6\ O_2\ G^o = 1.24\ V \qquad [1]$$

and

$$2H_2O \rightarrow 4H^+ + 4e^- + O_2\ G^o = 1.23\ V. \qquad [2]$$

The development of synthetic catalysts that can mediate water oxidation under mild conditions with a minimal energy cost has become an appealing challenge for chemists (3–7). Among various approaches, homogeneous molecular catalysts have shown attractive features such as controllable redox properties, ease of investigating reaction mechanisms, and strategies for the characterization of reactive intermediates (8, 9). Recently, such efforts have resulted in the development of a significant number of systems based on single-site and multinuclear transition metal complexes including Mn, Fe, Co, Cu, Ru, and Ir (9–15). Examples of cobalt-based molecular catalysts include a cobalt phthalocyanine (16), a cobalt "hangman" corrole (17), multipyridine cobalt complexes (18, 19), a dinuclear Co-peroxo species (20), and most recently, Co-porphyrins (21). Determining if these molecular complexes retain their homogenous nature during catalysis or merely act as precursors of truly active heterogeneous species such as films and nanoparticles has proven to be problematic (8, 22, 23). This scenario is especially critical for Co-based molecular catalysts because heterogeneous CoO_x species are highly active, so that even small amounts of this surface oxide layer could contribute significantly to the catalytic activity (24–27). Further, very little detailed mechanistic information for these systems is available to date, and the assignment of the key oxidants responsible for oxidizing a water molecule has been challenging (28). Here we describe mechanistic studies of a series of water-soluble, cationic cobalt porphyrins that effectively catalyze water oxidation electrochemically under mild conditions at neutral pH. The homogeneity of these catalysts was confirmed by a variety of techniques including electrochemical, spectroscopic, and surface analysis that exclude the alternative formation of heterogeneous cobalt oxide films. Our results indicate the generation of a reactive, high-valent Co^{IV}-porphyrin cation radical that has accumulated two oxidizing equivalents above the resting Co^{III} catalyst. Further, we demonstrate a critical role for the buffer base that accepts a proton during the O–O bond-formation event.

Results

The cobalt-porphyrin precursor, Co(II)–5,10,15,20-tetrakis-(1,3-dimethylimidazolium-2-yl) porphyrin tetrachloride (Co^{II}-TDMImP; Scheme 1) was prepared by metallation of the corresponding free base (29) and characterized by UV–vis, EPR, and mass spectroscopies. The UV–vis spectrum of Co^{II}-TDMImP showed a Soret band at 407 nm and two Q bands at 527 nm and 558 nm (*SI Appendix*, Fig. S1). The high-resolution electrospray mass spectrum

Significance

Efficient and scalable catalysts that mediate the interconversion of electrical and chemical energy are essential to the future world economy. Central to this challenge are robust systems that can split water into its elements, hydrogen and oxygen, with minimal cost. In this article, we describe the discovery and characterization of an efficient, single-site homogeneous water oxidation catalyst based on a cationic cobalt-porphyrin system. Important roles of the buffer base in this catalysis are also described. Our results shed light on the design of next-generation water oxidation catalysts using earth-abundant transition metals and redox active ligand systems.

Author contributions: D.W. and J.T.G. designed research; D.W. performed research; D.W. and J.T.G. analyzed data; and D.W. and J.T.G. wrote the paper.

The authors declare no conflict of interest.

[1]To whom correspondence should be addressed. E-mail: jtgroves@princeton.edu.

This article contains supporting information online at www.pnas.org/lookup/suppl/doi:10.1073/pnas.1315383110/-/DCSupplemental.

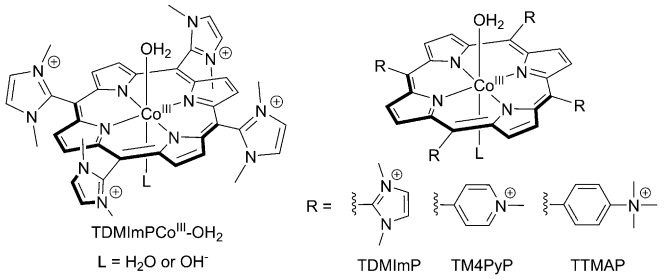

Scheme 1. Water-soluble cobalt porphyrins studied as water oxidation catalysts in this work.

exhibited an ion at a mass-to-charge ratio (m/z) of 186.82 (*SI Appendix*, Fig. S2), with the mass and isotope distribution patterns matching the calculated value (m/z = 186.82) for the quaternary ion [Co^{II}-TDMImP]$^{4+}$. The continuous-wave X-band EPR spectrum of Co^{II}-TDMImP showed a resonance at g_{eff} = 2.30 with partially resolved hyperfine splitting due to the nuclear spin of ^{59}Co (I = 7/2) (*SI Appendix*, Fig. S3, solid), indicating a low-spin Co^{II} center (S = 1/2). This signal is distinct from that of the free Co^{2+} ion measured under identical conditions (*SI Appendix*, Fig. S3, dotted line), which showed broad features at g_{eff} = 5.56 and 3.13 (30). Therefore, the amount of any free Co^{2+} salt as an impurity in the sample is very small. The 1-e$^-$ electrochemical oxidation of Co^{II}-TDMImP at an applied potential of 300 mV generated Co^{III}-TDMImP, the active form of the catalyst (described below), which showed red-shifted optical features at 419 nm (Soret band), 540 nm, and 575 nm (Q bands). The ^{1}H NMR spectrum (*SI Appendix*, Fig. S4) clearly indicated that Co^{III}-TDMImP is a diamagnetic species, as expected, with sharp resonances assignable to the porphyrin β-pyrrole protons, the imidazolium C4 and C5 protons, and the methyl protons at δ = 9.34, 8.12, and 3.67 ppm, respectively. The X-band EPR spectrum showed that Co^{III}-TDMImP was EPR silent (*SI Appendix*, Fig. S3, dashed), with negligible Co^{II} species present. Taken together, these results indicate that both Co^{II}-TDMImP and Co^{III}-TDMImP had been prepared in high purity (>99%). There was no evidence of Na–Pi buffer binding to either Co^{II}-TDMImP or Co^{III}-TDMImP at pH 7 (*SI Appendix*, Fig. S5).

A strong catalytic current with an onset potential of ∼1.2 V was observed in the cyclic voltammogram (CV) of 1 mM Co^{II}-TDMImP carried out in 0.2 M aqueous sodium phosphate (Na–Pi) at pH 7 (Fig. 1*A*, red trace). This feature, which was absent in scans of solutions containing buffer alone (Fig. 1*A*, black trace), showed a strong, linear dependence on the concentration of catalyst (Fig. 1*A*, *Inset*). Co^{II}-TDMImP (0.5 mM, pH 7) was then subjected to controlled potential bulk electrolysis at 1.30 V using an indium tin oxide (ITO) working electrode, while monitoring O_2 evolution with a Clark electrode. The rate constant (k_{obs}) of the O_2 formation was determined to be 1.4 × 10^3 s^{-1}, which is ∼18-fold larger than that reported by Berlinguette and coworkers (19). [k_{obs} was determined using the equation $i_{cat}/i_{diff} = 2.24n(RTk_{obs}/F\nu)^{1/2}$, where i_{cat} is the catalytic current, i_{diff} is the diffusional current of the Co$^{III/II}$ couple, n = 4, and ν is the scan rate. A plot of i_{cat}/i_{diff} vs. $\nu^{1/2}$ gives a linear relationship with a slope of $2.24n(RTk_{obs}/F)^{1/2}$, where k_{obs} can be calculated.] The faradaic yield for oxygen production determined by these measurements for this Co-porphyrin was 85–90% (*SI Appendix*, Fig. S6).

Sustained electrocatalytic oxygen evolution was observed for several hours without significant loss of the catalytic current (*SI Appendix*, Fig. S7). Inspection of the well-defined UV–vis spectrum during and after the electrolysis indicated that loss of the Co-porphyrin chromophore was insignificant and that the catalyst inventory remained predominantly Co^{III}-TDMImP (>98%) throughout (*SI Appendix*, Fig. S8). The catalytic current decreased with increasing scan rate over a range of scan rates from 50 to 500 mV·s^{-1} (*SI Appendix*, Fig. S9). This result indicates a rate-limiting chemical step, likely O–O bond formation, that precedes subsequent peroxide oxidation to O_2 on the electrode surface (31). The CV of Co-TDMImP taken in D_2O showed a significantly smaller catalytic current (Fig. 1*A*, blue trace) compared with that obtained in H_2O, indicative of a solvent isotope effect [kinetic isotope effect (KIE) or equilibrium isotope effect (EIE)] of 2.8 [the KIE was calculated according to KIE = $k_{cat,H2O}/k_{cat,D2O} = (i_{cat,H2O}/i_{cat,D2O})^2$; see ref. 31].

We performed a number of controls to assess the possible formation of heterogeneous metal oxide films. First, the stability of the catalyst was probed under active water oxidation catalysis (WOC) reaction conditions by monitoring the characteristic visible spectrum of Co^{III}-TDMImP (Q bands at 540 and 575 nm). As can be seen in *SI Appendix*, Fig. S8, there was negligible decomposition (<2%) over a period of 4 h. We found that 1 mM Co-TDMImP produced a catalytic current similar to that of a heterogeneous cobalt oxide film derived from 0.2 mM $Co(NO_3)_2$ (Fig. 1*B*). Accordingly, at least 20% decomposition of Co-TDMImP would have been required to generate the observed

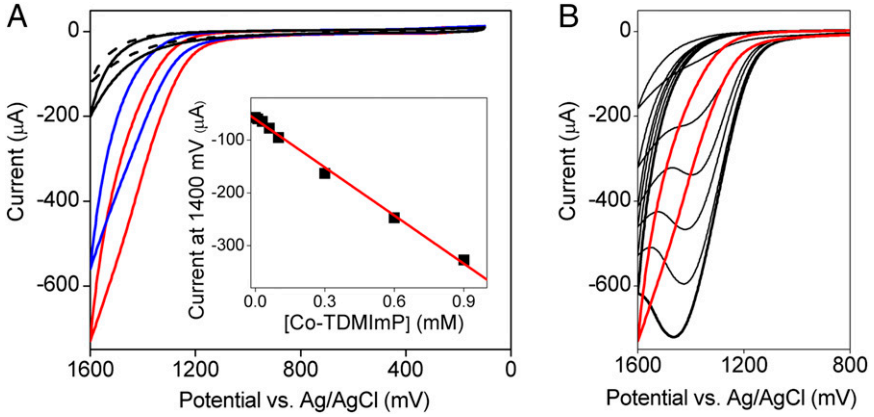

Fig. 1. WOC by Co-TDMImP and $Co(NO_3)_2$. (*A*) CVs of buffer background (black solid), 1 mM Co-TDMImP in H_2O (red) and in D_2O (blue), and clean buffer using the working electrode removed from 1 mM Co-TDMImP–containing solution after 20 CV scans (black dashed). (*A*, *Inset*) Plot of the catalytic current for Co-TDMImP at 1.40 V (Ag/AgCl) vs. [Co-TDMImP]. The red line represents the best linear fit. (*B*) CVs of 1 mM Co-TDMImP (red trace) and $Co(NO_3)_2$ (black traces) at concentrations (from top to bottom) of 0.01 mM, 0.05 mM, 0.1 mM, 0.13 mM, 0.17 mM, and 0.2 mM. Other conditions include glassy carbon working electrode, 0.2 M Na–Pi buffer, pH 7, 22 °C, and scan rate 100 mV·s^{-1}.

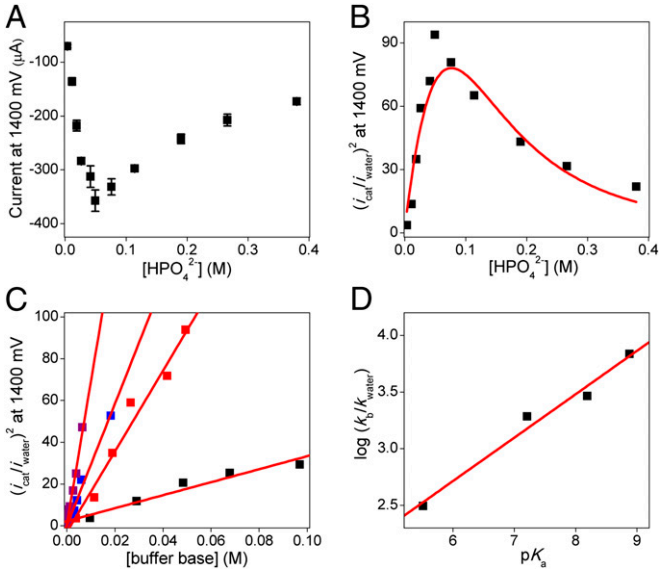

Fig. 2. Roles of the buffer anion in WOC. (*A*) Plot of the catalytic current for Co-TDMImP measured at 1.4 V vs. $[HPO_4^{2-}]$. (*B*) Plot of $(i_{cat}/i_{water})^2$ at 1.4 V vs. $[HPO_4^{2-}]$ and the best fit according to *SI Appendix*, Eq. **S3** (red). (*C*) Plot of $(i_{cat}/i_{water})^2$ at 1.4 V vs. the buffer dianion concentration; phthalate, black; Na–Pi, red; *n*-butylphosphonate, blue; *tert*-butylphosphonate, purple. (*D*) Plot of log (k_b/k_{water}) vs. pK_a of the buffer used and best linear fits (red). Other conditions include room temperature, scan rate 100 mV·s^{-1}, and pH 7.

current, which is completely inconsistent with this spectral monitoring. Likewise, linear sweep voltammetry showed that the catalytic activity of Co-TDMImP remained constant over this time (*SI Appendix*, Fig. S10). We next designed experiments using additives that would scavenge any free Co^{2+} ions present in the reaction medium. As illustrated in the *SI Appendix*, Fig. S11*A*, the addition of 0.25 mM EDTA completely suppressed the WOC activity of 0.2 mM $Co(NO_3)_2$. Further, no cobalt oxide film was observed to form on the electrode surface after multiple CV scans, whereas cobalt oxide was readily detected without added EDTA. In sharp contrast, the catalytic current observed for 1 mM Co-TDMImP retained its full intensity in the presence of 0.25 mM EDTA. These results indicate that there was no significant release of free Co^{2+} ions into the solution during catalysis in the presence of Co-TDMImP. This result also excludes the possibility that trace cobalt impurities in Co-TDMImP contribute to the observed WOC activity. Similar results were obtained using Chelex resin in a three-phase test. The addition of Chelex beads drastically reduced the observed catalytic current of 0.2 mM $Co(NO_3)_2$ sevenfold by sequestering free Co^{2+} ions (*SI Appendix*, Fig. S11B). However, the presence of Chelex beads had no effect on the observed WOC current with Co-TDMImP over the period of the measurement.

The onset potentials obtained using Co-TDMImP and $Co(NO_3)_2$ and the appearance of the catalytic waves are completely different (Fig. 1*B*). Further, there was no detectable lag phase in the development of catalytic current for the homogeneous cobalt-porphyrin system. When the working electrodes (both glassy carbon and ITO) were removed from the Co-porphyrin solutions after multiple CV scans or bulk electrolysis and used in clean buffers after gentle rinsing, no significant anodic current was observed relative to a freshly prepared electrode (Fig. 1*A* and *SI Appendix*, Fig. S7). Inspection of the surface morphology and composition of the glassy carbon electrodes by environmental scanning electron microscope (ESEM) and energy dispersive X-ray spectroscopy (EDX) analysis after multiple CV runs in Co-TDMImP solution with a concentration of even 5 mM showed clean surfaces with no sign of any heterogeneous cobalt phase (*SI Appendix*, Figs. S12 and S13). By contrast, an obvious cobalt-containing heterogeneous film formed on the electrode surface after scans in the same buffer solution containing as little as 0.1 mM $Co(NO_3)_2$. Accordingly, the release of any free Co^{2+} ions from Co-TDMImP must be less than 2% and not nearly enough to account for the large WOC current.

Several experiments were performed to examine the effects of the buffer concentration on the catalytic water oxidation activity. As shown in Fig. 2 and *SI Appendix*, Fig. S14, no catalytic activity was observed in unbuffered H_2O solution (pH ~7). However, a significant enhancement of the fixed-potential catalytic current, i_{cat}, was observed with increasing concentrations of HPO_4^{2-} buffer up to 60 mM. Care was taken during these measurements to maintain the ionic strength of the solution at 0.1 M with $NaNO_3$. Interestingly, a decrease of the catalytic current was observed when the concentration of the buffer base was increased beyond 60 mM (Fig. 3*A*). This observation suggests the presence of an inhibition pathway at high buffer concentrations. Besides Na–Pi ($pK_a = 7.21$), Co-TDMImP also catalyzed water oxidation at pH 7 with a variety of buffers, including phthalate ($pK_a = 5.51$), bicarbonate ($pK_a = 6.37$), *n*-butylphosphonate ($pK_a = 8.19$), and *tert*-butylphosphonate ($pK_a = 8.88$) (Figs. 2*C* and 3*A*).

No redox processes associated with the oxidation of Co^{III} or the porphyrin were observed by either CV or square wave voltammetry (SWV) for Co-TDMImP, presumably because any

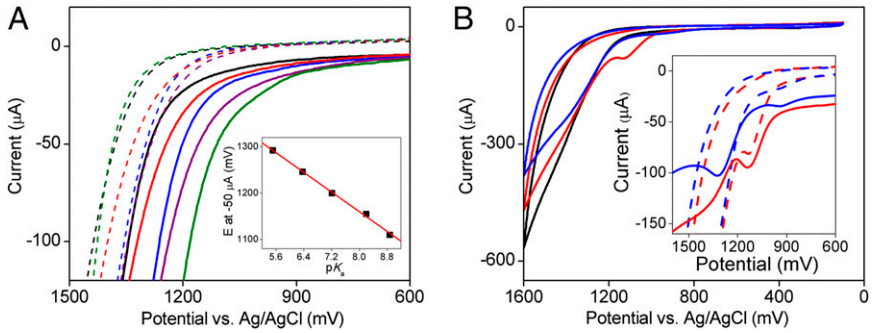

Fig. 3. Effect of the buffer anion on WOC onset potential and comparison of several cationic cobalt porphyrin WOC catalysts. (*A*) CVs of 1 mM Co-TDMImP in phthalate (black), bicarbonate (red), Na–Pi (blue), *n*-butylphosphonate (purple), and *tert*-butylphosphonate (green) buffers. The solid and dashed lines represent forward and backward scans, respectively. (*A*, *Inset*) Plot of the potential measured at –50 μA as a function of pK_a of the buffer species. The red line represents the best linear fit with a slope of –54 mV.pK_a^{-1}. (*B*) CVs of 1 mM Co-TDMImP (black), Co-TM4PyP (red), and Co-TTMAP (blue). (*B*, *Inset*) Amplified CVs (dashed lines) and SWVs (solid lines) of Co-TM4PyP (red) and Co-TTMAP (blue) showing the 600–1,400 mV range. Other conditions include room temperature, scan rate 100 mV·s^{-1}, and pH 7.

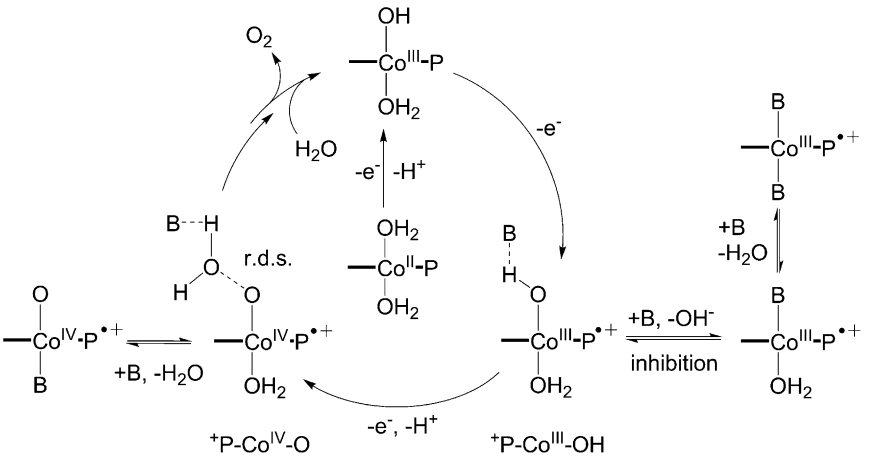

Scheme 2. Proposed mechanism for water oxidation catalyzed by Co-porphyrins involving two one-electron oxidations of Co^{III} to $^{+}$P-Co^{III}–OH and $^{+}$P-Co^{IV}–O. Roles for the buffer anion (B) include serving as a base to assist proton transfer and inhibition of the catalyst through coordination.

species more oxidized than Co^{III} are short lived. To gain more mechanistic insight, we compared the behavior of Co-TDMImP with two other water-soluble cationic Co-porphyrins, Co–5,10,15,20-tetrakis-(*N*-methylpyridinium-4-yl)porphyrin (TM4PyP) (32) and Co–5,10,15,20-tetrakis-(*N*,*N*,*N*-trimethylanilinium-4-yl)porphyrin (TTMAP) (Scheme 1). As shown in Fig. 3*B*, Co-TM4PyP and Co-TTMAP also catalyzed water oxidation under these conditions, but with diminished efficiency. The catalytic activity, as illustrated by the intensity of the catalytic current at a fixed potential (e.g., 1.50 V), decreased in the order of Co-TDMImP > Co-TM4PyP > Co-TTMAP. Accordingly, the reactive species generated in solutions of Co-TM4PyP and Co-TTMAP are apparently less potent oxidants of H_2O than that of Co-TDMImP. Notably, anodic waves were observed at 1,130 mV and 920 mV in the CVs of Co-TM4PyP and Co-TTMAP, respectively (Fig. 3*B*, *Inset*).

To illuminate the redox properties of the porphyrin ring, we examined the electrochemical behavior of the corresponding Ga^{III}-porphyrins. A single oxidative process was observed at 1,140 mV and 930 mV for Ga^{III}-TM4PyP and Ga^{III}-TTMAP, respectively, both by CV and SWV (*SI Appendix*, Fig. S15). For Ga^{III}-TDMImP, a broad anodic feature was observed at ∼1,380 mV. These oxidative waves were insensitive to the pH of the solution. Bulk electrolytic oxidation of these Ga^{III} porphyrins afforded a species with an absorption feature centered in a range of 650–660 nm, typical of a porphyrin radical cation (33, 34). Furthermore, the oxidation potential of Ga^{III}-TM4PyP (1,140 mV) is similar to that of $(O)Fe^{IV}$-TM4PyP, which generates the known oxoiron porphyrin cation radical (34, 35).

An additional oxidative wave beyond the oxidation of the porphyrin was observed at 1,320 mV for Co-TTMAP by SWV (Fig. 3*B*, *Inset*). This feature was not elicited in the CV, as it lies under the catalytic current, indicating that this wave represents the generation of the reactive oxidant that mediates H_2O oxidation catalysis. Moreover, similar to Co-TDMImP, a dependence of the onset potential on the pK_a of the buffer base was also observed (*SI Appendix*, Fig. S16). The second oxidation of Co-TM4PyP was less resolved but still evident in the SWV (Fig. 3*B*, *Inset*), whereas this feature could not be observed for Co-TDMImP. Presumably, the oxidized species of the latter two Co-porphyrins are too reactive to accumulate.

Discussion

The results show that the electron-deficient cobalt porphyrin, Co-TDMImP, is an efficient catalyst for the electrochemical oxidation of water to oxygen. The onset potential of ∼1.2 V (Fig. 1*A*) compares favorably with values reported for other cobalt-based catalysts, whereas the catalytic current appears to be significantly greater than those of other systems (17, 25). The observed O_2 formation rate, 170 nmol·cm^{-2}·min^{-1}, is much higher than that of a recently described iridium-based homogeneous catalyst (36), and the 85–90% faradaic yield for oxygen production indicates nearly exclusive 4-e$^-$ oxidation of H_2O (*SI Appendix*, Fig. S6).

Several lines of evidence show that this is clearly a homogeneous system. In particular, the stability of the resting Co^{III} complex over hours of measurement and the lack of any effects on catalytic efficiency by either cobalt ion sequestration with EDTA or a three-phase test with Chelex resin show that free cobalt ions are not contributing to the observed WOC activity. This conclusion is further confirmed by the lack of any sign of heterogeneous surface films on the electrodes. Moreover, indications from the scan-rate dependence that O–O bond formation is rate limiting and the strictly linear dependence of catalytic current on catalyst concentration argue that Co-TDMImP is a single-site, molecular catalyst.

The titration of two acidic protons in $Co^{III}(OH_2)_2$-TDMImP (pK_a = 5.1 and 9.4; *SI Appendix*, Fig. S1) and the measured $Co^{III/II}$ potential at 250 mV (ΔE = 100 mV) vs. Ag/AgCl reference (*SI Appendix*, Figs. S5 and S17) indicate that the resting state of the Co-TDMImP catalyst at pH 7 is H_2O–Co^{III}–OH. The $Co^{III/II}$ redox potential (250 mV; *SI Appendix*, Fig. S17) of Co-TDMImP is higher than that of Co-TM4PyP and Co-TTMAP; however, it is still too low for the exchange labile Co^{II} state to be involved in catalysis. This conclusion could explain why Co-TDMImP does not lose cobalt ions during catalysis.

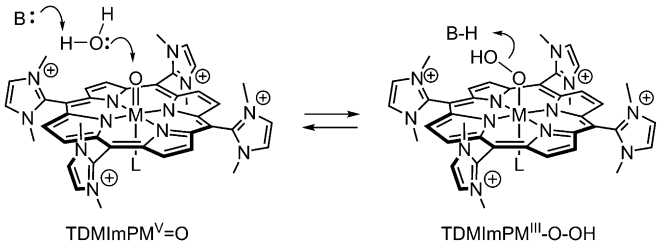

Scheme 3. Proposed pathways for O–O bond formation and cleavage catalyzed by cobalt and manganese metalloporphyrins bearing the electron withdrawing TDMImP ligand.

The cyclic voltammetry and square wave electrochemical results for the family of cobalt and gallium porphyrins studied indicate that porphyrin ring oxidation was occurring at potentials at or below the onset potential for water oxidation. This behavior was most clearly evident for Ga^{III}- and Co^{III}-TM4PyP, which showed ring oxidations at 1.14 and 1.13 V, respectively. Bulk spectroelectrochemical analysis of Ga^{III}-TM4PyP showed a typical, broad, porphyrin radical cation absorbance in the visible spectrum ~660 nm.

These experimental findings strongly indicate that the observed anodic features ~1 V vs. Ag/AgCl represent ligand oxidations to the corresponding porphyrin radical cations. No other oxidation waves were observed for the Ga^{III} porphyrins, indicating that the formation of porphyrin dications is not likely. More importantly, oxidation potentials of Ga^{III}-TM4PyP and Ga^{III}-TTMAP are almost identical to those observed for Co^{III}-TM4PyP and Co^{III}-TTMAP (Fig. 3*B* and *SI Appendix*, Fig. S15). Therefore, we conclude that the oxidative wave found in CVs of these Co-porphyrins also represents the oxidation of Co^{III} porphyrin to the Co^{III} porphyrin radical cation ($^{+}$P-Co^{III}–OH). Because the observed ring oxidations occurred before the onset of the WOC catalytic current, the $^{+}$P-Co^{III}–OH is not the reactive oxidant in this system. The second anodic oxidation, beyond that of the porphyrin ring, which was observed at 1,320 mV for Co-TTMAP by SWV (Fig. 3*B*, *Inset*), appeared to coincide with water oxidation. We suggest that this process represents a 1-e^{-} oxidation of the $^{+}$P-Co^{III}–OH coupled with the loss of one proton to the buffer anion to generate a Co^{IV}–O porphyrin radical cation ($^{+}$P-Co^{IV}–O). Thus, the formally cobalt(V) species that is catalytically competent for WOC has accumulated two oxidation equivalents above Co^{III}. Subsequent, rate-limiting O–O bond formation at a single cobalt site is supported by the scan-rate dependence of the catalytic current and the linear dependence of the catalytic current on the catalyst concentration.

Considering the results above, we propose a mechanism for Co-porphyrin-mediated water oxidation as shown in Scheme 2. The generation of the reactive oxidant, $^{+}$P-Co^{IV}–O, requires the transfer of two electrons and one proton from the resting (aqua) Co^{III}–OH complex. The first oxidation, which is pH independent, would generate $^{+}$P-Co^{III}–OH, which then must undergo a second oxidation at the cobalt center, with loss of a single proton. The key O–O bond formation step involves nucleophilic addition of H_2O to $^{+}$P-Co^{IV}–O to generate a presumed Co-hydroperoxo or peroxo intermediate that is further oxidized to produce O_2. Recently, a Co^{IV}–O–containing unit was characterized in a catalytic H_2O oxidation system mediated by a heterogeneous cobalt oxide catalyst (37). Likewise, a Co^{IV}-corrole cation radical was proposed as the active species by Nocera and coworkers for the hangman systems (17). This hypothetical intermediate has been investigated by Lai et al. using density function theory (DFT) computational methods (38). This work indicated that O–O bond formation in an oxoCo^{IV}-corrole cation radical was the most exothermic reaction with the lowest activation barrier (3.6 kcal/mol) among a number of intermediates studied. The data presented here provide experimental support for such a pathway in the cobalt-porphyrin platform. The single-site aspect of the WOC cycle in Scheme 2 and the critical role of porphyrin ring oxidation contrast to the cobalt-oxyl dimerization pathway were recently suggested by Sakai and coworkers for a photocatalytic cobalt-porphyrin water oxidation that used a peroxide as a sacrificial oxidant (21).

The nucleophilic addition of water to a doubly oxidized cobalt-oxo intermediate is formally the microscopic reverse of the conversion of the manganese analog HOO-Mn^{III}TDMImP to *trans*-dioxoMn^{V}TDMImP that we have recently described (Scheme 3) (39, 40). Here, both the hydroperoxo–manganese(III) complex and the oxo–manganese(V) complex were spectroscopically observed and the kinetics of the process could be analyzed in detail. Significantly, the activation enthalpy of the O–O bond cleavage event was determined to be only 4.2 kcal/mol despite the large-scale reorganization that seems to be required for such a transformation. Likewise, reaction of chloride ion with *trans*-dioxo-Mn^{V}TDMImP to form hypochlorite via an analogous O–Cl bond formation was shown to be fast and reversible (41, 42). Redox potential determinations and Nernst equation considerations showed that the potential of this Mn^{V}/Mn^{III} porphyrin system was poised only 100–200 mV below the hydrogen peroxide/water couple. Thus, the high potentials of the electron-deficient TDMImP porphyrin ring oxidation and that expected for the Co^{IV}/Co^{III} couple have apparently crossed that threshold.

An important aspect of the current work is the prominent effect of the buffer anion on cobalt WOC. No water oxidation was observed in the absence of the buffer in this aqueous medium at constant ionic strength. For such a base-assisted process, the overall O–O bond formation rate (k_{cat}) can be expressed by the sum of the rate in unbuffered solution (k_{water}) and the rate contributed by the addition of buffer base (k_b[B]), as shown in Eq. **3** (31, 43). Thus, a plot of $(i_{cat}/i_{water})^2$ as a function of the buffer base concentration [B] should give a linear correlation with an intercept close to 1 and a slope equal to k_b/k_{water} (Eq. **4**). Indeed, this prediction was observed experimentally (Fig. 2*B*, red filled squares), indicating that one equivalent of buffer base is involved in the rate-limiting O–O bond formation step:

$$k_{cat} = k_{water} + k_b[B] \quad \textbf{[3]}$$

and

$$(i_{cat}/i_{water})^2 = k_{cat}/k_{water} = 1 + k_b[B]/k_{water}. \quad \textbf{[4]}$$

As shown in Fig. 2*C*, the $(i_{cat}/i_{water})^2$ value showed a linear dependence on the concentration of each buffer base. Notably, a Brønsted relationship could be discerned between log (k_b/k_{water}) and the pK_a of the buffer used (Fig. 2*D*). The slope of 0.38 is a further indication that there is a significant component of proton transfer from the catalyst to the buffer anion in the transition state for the rate-limiting O–O bond formation step (44). We were able to fit the observed biphasic behavior of WOC activity over the entire range of buffer concentrations studied for the four buffers used (*SI Appendix*, Fig. S18 and Table S1) by assuming that multiple equilibria are involved in the inhibition pathway (*SI Appendix*, *Data Fitting for Details*). Interactions of both the –OH ligand on $^{+}$P–Co^{III}–OH and a H_2O ligand with a buffer anion are necessary to get the best fit. The latter could occur at either the Co^{III} or Co^{IV} porphyrin cation radical stage (Scheme 2).

The nature of the buffer also affected the onset potential of WOC. As shown in Fig. 3*A*, the onset potential at pH 7 decreased significantly in solutions containing more basic buffer anions; the lowest onset potential was found in the *tert*-butylphosphonate buffer, which has the highest pK_a among the five buffers used. Importantly, a plot of the potential measured at a fixed current (–50 μA) as a function of pK_a of the buffer used gave a linear correlation with a slope of –54 mV·pK_a^{-1}, indicating clearly that the generation of the reactive oxidant that effects WOC requires the removal of one proton from the precursor (43). In this PCET process (45), the electron transfer (ET) part appears to become more favorable, as illustrated by the negative shift of the onset potential, when the PT component is facilitated by the presence of a more basic buffer anion.

The data indicate that the buffer base must play multiple roles in the catalytic cycle (Scheme 2), including (*i*) acting as a proton acceptor in the conversion of the $^{+}$P–Co^{III}–O–H intermediate to the doubly oxidized $^{+}$P-Co^{IV}–O precursor of WOC; (*ii*) acting as a base to deprotonate water coupled with the rate-limiting O–O bond formation step, consistent with a KIE (or EIE) value of 2.8 measured

in H_2O vs. in D_2O; and (*iii*) inhibiting catalytic water oxidation activity at high buffer concentrations. Buffer anion catalysis of the O–O bond formation step and buffer inhibition has been reported for a homogeneous, single-site ruthenium water oxidation catalyst system developed by Meyer, et al. (31), and it has been postulated that the pendant carboxylate moiety of the cobalt hangman corrole acts as a general base to assist the O–O bond formation by mediating the transfer of a proton from a water molecule (17, 38).

In summary, water-soluble cationic Co-porphyrins are effective homogeneous water oxidation electrocatalysts that function at neutral pH and a modest overpotential. Co-TDMImP, which was the best catalyst, was robust during catalysis and was not a precursor of a heterogeneous cobalt oxide film. Mechanistic studies indicate that a high-valent Co-porphyrin, presumably a Co^{IV}–O porphyrin radical cation, is the reactive oxidant responsible for attacking a H_2O molecule to form the O–O bond. Accordingly, the catalysis proceeds through a $Co^{V/III}$ cycle that would guarantee high activity, while minimizing catalyst decomposition by avoiding the exchange labile Co^{II} state. Co-TDMImP, the most electron-deficient complex having the highest redox potential, was the best catalyst among the three Co-porphyrins studied. Accordingly, the reactive oxidant has a higher oxidation potential than those of Co-TM4PyP and Co-TTMAP, providing a more thermodynamic driving force for water oxidation. The buffer base has been demonstrated to play multiple, critical roles during catalysis.

The dramatic effect of the buffer pK_a on the WOC onset potential is worthy of special note. Significantly, water oxidation began near 1 V with the most basic phosphonate buffer anion. This observation is very informative and suggests that a WOC catalyst with properly positioned internal phosphonates could provide the necessary proton transfer catalysis without the inhibitory effects observed at high buffer concentrations. These considerations are informing our continuing studies of next-generation WOC catalysts using earth-abundant transition metals.

ACKNOWLEDGMENTS. We thank the Princeton Institute for the Science and Technology of Materials and Dr. Shiyou Xu for the help of ESEM and EDX analyses. Support of this research by the National Science Foundation (CHE-1148597) is gratefully acknowledged. Electrocatalysis was supported by the Center for Catalytic Hydrocarbon Functionalization (CCHF), an Energy Frontier Research Center, US Department of Energy, Office of Science, Basic Energy Sciences, under Award DE-SC0001298.

1. Barber J (2009) Photosynthetic energy conversion: Natural and artificial. *Chem Soc Rev* 38(1):185–196.
2. McEvoy JP, Brudvig GW (2006) Water-splitting chemistry of photosystem II. *Chem Rev* 106(11):4455–4483.
3. Concepcion JJ, House RL, Papanikolas JM, Meyer TJ (2012) Chemical approaches to artificial photosynthesis. *Proc Natl Acad Sci USA* 109(39):15560–15564.
4. Faunce TA, et al. (2013) Energy and environment policy case for a global project on artificial photosynthesis. *Energy Environ Sci* 6(3):695–698.
5. Faunce T, et al. (2013) Artificial photosynthesis as a frontier technology for energy sustainability. *Energy Environ Sci* 6(4):1074–1076.
6. Dau H, et al. (2010) The mechanism of water oxidation: From electrolysis via homogeneous to biological catalysis. *Chemcatchem* 2(7):724–761.
7. Helm ML, Stewart MP, Bullock RM, DuBois MR, DuBois DL (2011) A synthetic nickel electrocatalyst with a turnover frequency above 100,000 s^{-1} for H_2 production. *Science* 333(6044):863–866.
8. Artero V, Fontecave M (2013) Solar fuels generation and molecular systems: Is it homogeneous or heterogeneous catalysis? *Chem Soc Rev* 42(6):2338–2356.
9. Wasylenko DJ, Palmer RD, Berlinguette CP (2013) Homogeneous water oxidation catalysts containing a single metal site. *Chem Commun (Camb)* 49(3): 218–227.
10. Sartorel A, Bonchio M, Campagna S, Scandola F (2013) Tetrametallic molecular catalysts for photochemical water oxidation. *Chem Soc Rev* 42(6):2262–2280.
11. Hetterscheid DGH, Reek JNH (2012) Mononuclear water oxidation catalysts. *Angew Chem Int Ed Engl* 51(39):9740–9747.
12. Concepcion JJ, et al. (2009) Making oxygen with ruthenium complexes. *Acc Chem Res* 42(12):1954–1965.
13. Ellis WC, McDaniel ND, Bernhard S, Collins TJ (2010) Fast water oxidation using iron. *J Am Chem Soc* 132(32):10990–10991.
14. Fillol JL, et al. (2011) Efficient water oxidation catalysts based on readily available iron coordination complexes. *Nat Chem* 3(10):807–813.
15. Codolà Z, et al. (2013) Electronic effects on single-site iron catalysts for water oxidation. *Chemistry* 19(25):8042–8047.
16. Abe T, et al. (2006) An organic photoelectrode working in the water phase: Visible-light-induced dioxygen evolution by a perylene derivative/cobalt phthalocyanine bilayer. *Angew Chem Int Ed Engl* 45(17):2778–2781.
17. Dogutan DK, McGuire R, Jr., Nocera DG (2011) Electocatalytic water oxidation by cobalt(III) hangman β-octafluoro corroles. *J Am Chem Soc* 133(24):9178–9180.
18. Leung C-F, et al. (2012) A cobalt(II) quaterpyridine complex as a visible light-driven catalyst for both water oxidation and reduction. *Energy Environ Sci* 5(7):7903–7907.
19. Wasylenko DJ, Ganesamoorthy C, Borau-Garcia J, Berlinguette CP (2011) Electrochemical evidence for catalytic water oxidation mediated by a high-valent cobalt complex. *Chem Commun (Camb)* 47(14):4249–4251.
20. Rigsby ML, et al. (2012) Cobalt analogs of Ru-based water oxidation catalysts: Overcoming thermodynamic instability and kinetic lability to achieve electrocatalytic O_2 evolution. *Chem Sci* 3(10):3058–3062.
21. Nakazono T, Parent AR, Sakai K (2013) Cobalt porphyrins as homogeneous catalysts for water oxidation. *Chem Commun (Camb)* 49(56):6325–6327.
22. Crabtree RH (2012) Resolving heterogeneity problems and impurity artifacts in operationally homogeneous transition metal catalysts. *Chem Rev* 112(3):1536–1554.
23. Widegren JA, Finke RG (2003) A review of the problem of distinguishing true homogeneous catalysis from soluble or other metal-particle heterogeneous catalysis under reducing conditions. *J Mol Catal A* 198(1-2):317–341.
24. Stracke JJ, Finke RG (2011) Electrocatalytic water oxidation beginning with the cobalt polyoxometalate $[Co_4(H_2O)_2(PW_9O_{34})_2]^{10-}$: Identification of heterogeneous CoO_x as the dominant catalyst. *J Am Chem Soc* 133(38):14872–14875.
25. Wasylenko DJ, Palmer RD, Schott E, Berlinguette CP (2012) Interrogation of electrocatalytic water oxidation mediated by a cobalt complex. *Chem Commun (Camb)* 48(15):2107–2109.
26. Natali M, et al. (2012) Is $[Co_4(H_2O)_2(\alpha\text{-}PW_9O_{34})_2]^{(10-)}$ a genuine molecular catalyst in photochemical water oxidation? Answers from time-resolved hole scavenging experiments. *Chem Commun (Camb)* 48(70):8808–8810.
27. Hong D, et al. (2012) Water-soluble mononuclear cobalt complexes with organic ligands acting as precatalysts for efficient photocatalytic water oxidation. *Energy Environ Sci* 5(6):7606–7616.
28. Artero V, Chavarot-Kerlidou M, Fontecave M (2011) Splitting water with cobalt. *Angew Chem Int Ed Engl* 50(32):7238–7266.
29. Tjahjono DH, Akutsu T, Yoshioka N, Inoue H (1999) Cationic porphyrins bearing diazolium rings: Synthesis and their interaction with calf thymus DNA. *Biochim Biophys Acta* 1472(1-2):333–343.
30. McAlpin JG, et al. (2010) EPR evidence for Co(IV) species produced during water oxidation at neutral pH. *J Am Chem Soc* 132(20):6882–6883.
31. Chen Z, et al. (2010) Concerted O atom-proton transfer in the O-O bond forming step in water oxidation. *Proc Natl Acad Sci USA* 107(16):7225–7229.
32. Kellett RM, Spiro TG (1985) Cobalt (I) porphyrin catalysis of hydrogen production from water. *Inorg Chem* 24(15):2373–2377.
33. Groves JT, Haushalter RC, Nakamura M, Nemo TE, Evans BJ (1981) High-valent iron-porphyrin complexes related to peroxidase and cytochrome P450. *J Am Chem Soc* 103(10):2884–2886.
34. Bell SR, Groves JT (2009) A highly reactive p450 model compound I. *J Am Chem Soc* 131(28):9640–9641.
35. Lei J, Ju H, Ikeda O (2004) Catalytic oxidation of nitric oxide and nitrite mediated by water-soluble high-valent iron porphyrins at an ITO electrode. *J Electroanal Chem* 567(2):331–338.
36. Schley ND, et al. (2011) Distinguishing homogeneous from heterogeneous catalysis in electrode-driven water oxidation with molecular iridium complexes. *J Am Chem Soc* 133(27):10473–10481.
37. Surendranath Y, Kanan MW, Nocera DG (2010) Mechanistic studies of the oxygen evolution reaction by a cobalt-phosphate catalyst at neutral pH. *J Am Chem Soc* 132(46):16501–16509.
38. Lai WZ, et al. (2012) Why is cobalt the best transition metal in transition-metal hangman corroles for O-O bond formation during water oxidation? *J Phys Chem Lett* 3(17):2315–2319.
39. Jin N, Lahaye DE, Groves JT (2010) A "push-pull" mechanism for heterolytic O-O bond cleavage in hydroperoxo manganese porphyrins. *Inorg Chem* 49(24):11516–11524.
40. Lahaye D, Groves JT (2007) Modeling the haloperoxidases: Reversible oxygen atom transfer between bromide ion and an oxo-Mn(V) porphyrin. *J Inorg Biochem* 101(11-12):1786–1797.
41. Umile TP, Groves JT (2011) Catalytic generation of chlorine dioxide from chlorite using a water-soluble manganese porphyrin. *Angew Chem Int Ed Engl* 50(3):695–698.
42. Umile TP, Wang D, Groves JT (2011) Dissection of the mechanism of manganese porphyrin-catalyzed chlorine dioxide generation. *Inorg Chem* 50(20):10353–10362.
43. Bard AJ, Faulkner LR (2001) Electrode reactions with coupled homogeneous chemical reactions. *Electrochemical Methods: Fundamentals and Applications*, ed Harris D (Wiley, Hoboken, NJ), pp 471–534.
44. Ansyln EV, Dougherty DA (2006) *Modern Physical Organic Chemistry* (University Science Books, Sausalito, CA).
45. Weinberg DR, et al. (2012) Proton-coupled electron transfer. *Chem Rev* 112(7): 4016–4093.